AIP Applied Physics Letters

Effect of chromium underlayer on the properties of nano-crystalline diamond films

E. Garratt, S. AlFaify, T. Yoshitake, Y. Katamune, M. Bowden et al.

Citation: Appl. Phys. Lett. **102**, 011913 (2013); doi: 10.1063/1.4774086
View online: http://dx.doi.org/10.1063/1.4774086
View Table of Contents: http://apl.aip.org/resource/1/APPLAB/v102/i1
Published by the American Institute of Physics.

Related Articles

Synthesis and magnetostrictive properties of Pr(Fe1.95B0.05)1.93 bulk nanocrystalline alloy
Appl. Phys. Lett. 101, 192405 (2012)

New oxyfluoride glass with high fluorine content and laser patterning of nonlinear optical BaAlBO3F2 single crystal line
J. Appl. Phys. 112, 093506 (2012)

Tribological properties of nanocrystalline diamond films deposited by hot filament chemical vapor deposition
AIP Advances 2, 032164 (2012)

Magnetism and structure of graphene nanodots with interiors modified by boron, nitrogen, and charge
J. Chem. Phys. 137, 054715 (2012)

Surface fingerprints of individual silicon nanocrystals in laser-annealed Si/SiO2 superlattice: Evidence of nanoeruptions of laser-pressurized silicon
J. Appl. Phys. 111, 124302 (2012)

Additional information on Appl. Phys. Lett.

Journal Homepage: http://apl.aip.org/
Journal Information: http://apl.aip.org/about/about_the_journal
Top downloads: http://apl.aip.org/features/most_downloaded
Information for Authors: http://apl.aip.org/authors

ADVERTISEMENT

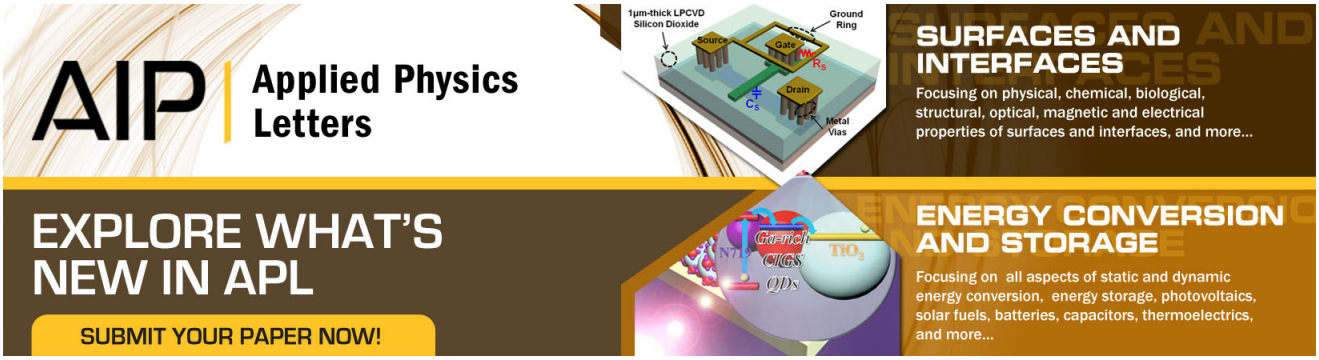

Effect of chromium underlayer on the properties of nano-crystalline diamond films

E. Garratt,[1] S. AlFaify,[1,2] T. Yoshitake,[3] Y. Katamune,[3] M. Bowden,[4] M. Nandasiri,[1,4] M. Ghantasala,[5] D. C. Mancini,[6] S. Thevuthasan,[4] and A. Kayani[1]
[1]*Department of Physics, Western Michigan University, Kalamazoo, Michigan 49008, USA*
[2]*Physics Department, King Khalid University, Abha, Saudi Arabia*
[3]*Department of Applied Science for Electronics and Materials, Kyushu University, Fukuoka 816-8580, Japan*
[4]*EMSL, Pacific Northwest National Laboratory, Richland, Washington 99354, USA*
[5]*Department of Mechanical and Aeronautical Engineering, Western Michigan University, Kalamazoo, Michigan 49008, USA*
[6]*Physical Sciences and Engineering, Argonne National Laboratory, Argonne, Illinois 60439, USA*

(Received 19 October 2012; accepted 18 December 2012; published online 11 January 2013)

This paper investigated the effect of chromium underlayer on the structure, microstructure, and composition of the nano-crystalline diamond films. Nano-crystalline diamond thin films were deposited at high temperature in microwave-induced plasma diluted with nitrogen, on single crystal silicon substrate with a thin film of chromium as an underlayer. Characterization of the film was implemented using non-Rutherford backscattering spectrometry, Raman spectroscopy, near-edge x-ray absorption fine structure, x-ray diffraction, and atomic force microscopy. Nanoindentation studies showed that the films deposited on chromium underlayer have higher hardness values compared to those deposited on silicon without an underlayer. Diamond and graphitic phases of the films evaluated by x-ray and optical spectroscopic analyses determined consistency between the sp^2 and sp^3 phases of carbon in chromium sample to that of diamond grown on silicon. Diffusion of chromium was observed using ion beam analysis which was correlated with the formation of chromium complexes by x-ray diffraction. © *2013 American Institute of Physics*. [http://dx.doi.org/10.1063/1.4774086]

Diamond and diamond-like thin films are important for technological applications ranging from microelectronics to tribologics.[1,2] The realization of nano- and ultrananocrystalline diamond (NCD and UNCD) films has enhanced the efficacy of diamond films in the fields of microelectromechanical, optical, and other devices.[3,4] The average grain size of these films ranges from tens to hundreds of nanometers, with the volume of graphitic sp^2 bonding reduced to 10% in UNCD.[5]

Research has shown that the characteristics of NCD/UNCD films, typically grown using microwave plasma chemical vapor deposition (MPCVD), change through manipulation of the relative concentrations of ionized gases and modifications to the growth surface.[6,7] For example, films grown on an underlayer of tungsten and molybdenum have displayed a higher nucleation density and smoother surfaces than those prepared by traditional seeding methods.[8,9] Based on the choice of underlayer, one can also enhance interfacial cohesiveness of resultant films,[10] clearly demonstrating that the choice of underlayer can have a significant effect on the properties of deposited films. Studies have shown that films grown on different underlayers produce interesting structures[11] or compounds,[12] whose overall effect may enhance or become a detriment[13] to the system. To tailor the characteristics of such systems, various metallic underlayers have been used.[14–16] Among these, chromium has been used as interfacial barriers between the iron and carbon during deposition to prevent the formation of graphitic phase film[17] and was shown to lead to the formation of useful microstructures in diamond films; i.e., mechanical interlocking of diamond grains into chromium carbides on steel substrates.[18] As chromium has been used as an adhesive layer on different substrates during the fabrication of many micro and nano devices, it was chosen as an underlayer.

In this study, a nano-crystalline diamond film deposited on a thin chromium layer over silicon at high substrate temperature has been fully characterized. Though chromium has been used as an underlayer during radio frequency chemical vapor deposition (RFCVD) of DLC coatings,[19] no similar study has been done on NCD. The NCD films, in this study, were deposited in a MPCVD system, within nitrogen diluted atmosphere. The presence of nitrogen provides growth enhancements of smoothness and morphology.[20–22] This study compares the properties of the NCD films grown on a chromium underlayer to a control sample grown on silicon and ascertains the effect of this underlayer on NCD film properties, characterizing composition, structure, microstructure, and interfacial characteristics.

NCD thin films were deposited on silicon substrates with and without a chromium underlayer using a MPCVD system (Lambda Technology, USA) at center for the nanoscale materials (CNM), Argonne National Laboratory. Prior to film growth, a chromium layer of approximately 50 nm was deposited on silicon using magnetron sputtering physical vapor deposition (PVD). Coated substrates were then transferred from the PVD chamber to the CVD chamber in air for film growth. NCD films were grown in a gas mixture of argon, nitrogen, and methane, which were allowed into the deposition chamber at constant flow rates of 160, 40, and 3 sccm, respectively, with the total chamber pressure

 © 2013 American Institute of Physics

maintained at 80 mbar. The microwave power was kept constant at 2.3 kW, while the substrate temperature was held at 750 °C. The thicknesses of the resultant NCD films grown on silicon and a chromium underlayer, determined based on a target simulation of non-Rutherford backscattering spectrometry (NRBS) spectra by SIMNRA, were approximately 215 and 384 nm, respectively.

The NCD films were characterized using Raman spectroscopy and near-edge x-ray absorption fine structure (NEXAFS) to determine the molecular structure of the films. Raman spectroscopy was carried out using a Renishaw Via Reflex Raman microscope having a laser source at 633 nm wavelength. NEXAFS was performed in cooperation with Kyushu University, at the SAGA Light Source located in Tosu City, Kyushu, Japan. After passing synchrotron radiation through two 10 μm slits in beamline 12, the spectra of samples were recorded in total electron yield (TEY) mode in the energy range of 280–345 eV.

Ion beam analysis was performed using a 6 MV tandem Van de Graaff accelerator located at Western Michigan University. The carbon deposition profile was measured via NRBS. A 3.35 MeV alpha particle beam (diameter of 2 mm) was used in NRBS to obtain an enhanced cross section[23] with carbon. The backscattered ions were detected at a scattering angle of 160°. Total charge collected on the sample was 16 μC from a beam of 20 nA.

The structure and microstructure of these samples were analyzed using x-ray diffraction (XRD) and atomic force microscopy (AFM), respectively. XRD patterns were collected using a Rigaku D/Max Rapid II micro diffraction system. X-rays were generated from a rotating Cr target ($\lambda = 2.2910$ Å) and focused through a 300 μm diameter collimator onto the specimen surface, making an incident angle of approximately 10°. XRD data were recorded for a 2θ range of 10° to 160°. Phases present were identified using the International Committee for Diffraction Data (ICDD) JADE v9.3 software (Materials Data Inc., CA). AFM measurements were performed using a Pacific Nanotechnology SPM, Nano-R series, and scanning probe microscope under close contact mode. Nanoindentation tests were carried out to measure the hardness and Young's Modulus of each film. Measurements were performed using a Nanoindenter II machine located at the Electron Microbeam Analysis Laboratory, University of Michigan. Penetration depths using a Berkovich tip were limited to 100 nm or 20 mN of force. Elastic modulus and hardness were determined using the Oliver and Pharr method.[24]

Raman spectra of the NCD films grown on pure silicon substrate as well as with a chromium underlayer are shown in Figure 1. The peaks at 1370 and 1580 cm^{-1} are the *D* and *G* modes of sp^2-bonded carbon, respectively, while the peak at 1155 cm^{-1} corresponds to a trans-polyacetylene phase. The fourth peak at 520 cm^{-1} is due to the silicon substrate.[25,26] The D and G modes are attributed to the breathing and stretching of planar carbon at the grain boundaries of NCD.[27,28] Raman spectroscopy has been employed in the past to detect carbon structures within amorphous thin films.[29]

Raman spectra of the NCD films deposited on silicon substrate with and without a chromium underlayer were quite similar. Normalized spectra, shown as an inset in Figure 1, confirmed this further. I(D)/I(G) ratios taken from the peak maxima of each mode were also consistent at 0.50 and 0.52 for samples grown on silicon and chromium, respectively, indicating the fractional volume of the lattice structures associated with sp^2 carbon is also similar. These results indicate an overall consistency of graphitic and amorphous phases of carbon between samples deposited on silicon and chromium.

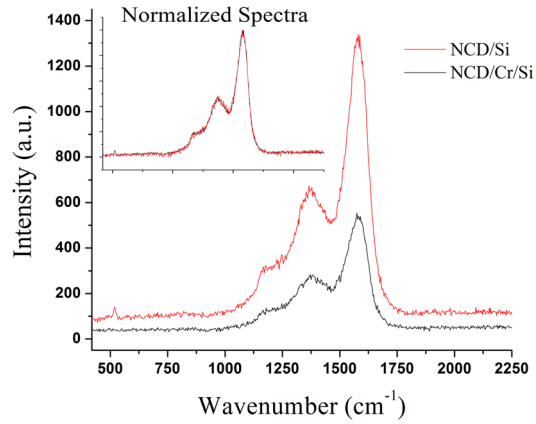

FIG. 1. Raman spectra for NCD samples grown on silicon (NCD/Si) and a chromium underlayer (NCD/Cr/Si).

Further, NEXAFS studies were performed to confirm the presence of diamond within the NCD sample grown on chromium coated silicon. NEXAFS is an excellent technique to study bond states due to the sensitivity being uninfluenced by grain sizes. The normalized absorption patterns of C1s transitions for both samples at photon energies between 280 and 315 eV are given in Figure 2. In the pre-edge region, a peak is visible at 284.5 eV, attributed to the C1s $\rightarrow \pi^*$ transition.[30] The absorption edge for diamond in both samples (C1s $\rightarrow \sigma^*$ transition) is located at approximately 288.5 eV. In order to confirm the shift of the absorption edge of diamond, observed within both samples, from 289.5 eV (Ref. 30), separate measurements were taken of (100) oriented nitrogen doped NCD in

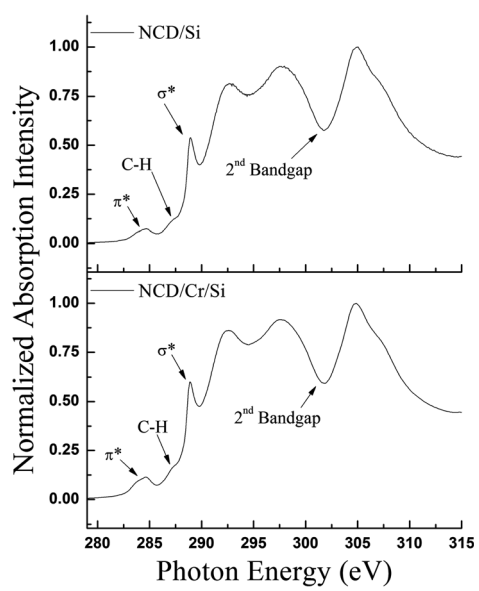

FIG. 2. NEXAFS spectrum for NCD on chromium coated and uncoated silicon.

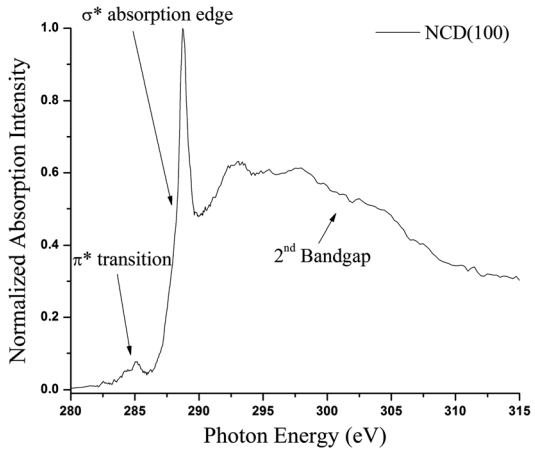

FIG. 3. NEXAFS spectrum for nanocrystalline (100) oriented diamond.

TEY (surface sensitive) mode (Figure 3). The diamond absorption edge of NCD was consistent with both the NCD on silicon and NCD on chromium coated silicon samples. A slight shift in the secondary bandgap associated with the σ^* exciton was also observed at 301.7 eV (from 302.5 eV) within the NEXAFS spectra of NCD samples. A peak at 287.2 eV, observed in both samples, has been assigned to different carbon bonding types under various conditions of sample preparation[31,32] and is likely due to carbon σ-type bonding with elements other than carbon.[33] Given the growth conditions and the presence of a trans-polyacetylene peak in both samples from Raman spectra, this peak is attributed to the σ^* transition for C-H.

To examine the relative differences between σ^* transition peaks associated with diamond in both samples, multiple peak fitting was performed. Figure 4 shows the fitted peak spectrum, which conforms closely to experimental data. The full width half maximum (FWHM) of the each σ^* transition peak was found to be: 0.58 for NCD/Cr/Si, 0.59 for NCD/Si, and 0.52 for NCD. Based on these values of the FWHM between each sample, there is relatively little difference in local electronic structure of sp^3 bond types. Additionally, the height differences between the π^* and σ^* absorption resonances of samples are about the same, indicating the relative yields from each volume of sp^2 and sp^3 carbon are about the same. Overall, the NEXAFS spectra confirmed the presence of sp^3 bond states within each film and indicated a relative consistency between films in terms of their localized electronic structure. Based on the characterizations from both Raman and NEXAFS measurements, the state of molecular carbon between the films is relatively unchanged.

XRD pattern of the films deposited on silicon substrate with and without chromium underlayer is shown in Figure 5. XRD patterns for NCD grown on silicon confirmed strong diamond (111) and (220) peaks at 2θ values 67.8° and 130°.[34] In contrast, the NCD carbon film deposited on a chromium underlayer showed a much more complex structure with many peaks in addition to diamond (111) and (220) phases. Interestingly, different peaks observed in this pattern were identified to belong to two additional phases of Cr-C-N and CrN. The peaks at 53.8°, 59.5°, 64.6°, and 69.8° associated with lattice planes of (111), (040), (211), and (131) are of Cr-C-N.[35] Similarly, the peaks at 57.2°, 67.1° (overlapping with (111) diamond), and 102.8° are identified to correspond to the lattice planes (111), (200), and (220) of CrN.[36] The formation of CrN and Cr-C-N phases may be explained by the diffusion of chromium/nitrogen during the high temperature growth of NCD. The presence of chromium oxide (Cr_2O_3) is evident by the occurrence of smaller peaks at 55.2° and 86.2°,[37] which may be attributed to atmospheric exposure of the chromium coating during loading into the CVD chamber. Possible interfacial interaction between the layers NCD and chromium, and chromium and silicon (substrate) seem to have resulted in the formation of these multiple polycrystalline phases compared to the pure diamond phases observed for the film deposited on silicon substrate.

In order to understand the interfacial mixing effects at the chromium, carbon, and silicon interfaces, NRBS analysis was performed on these samples. The path of the ion beam

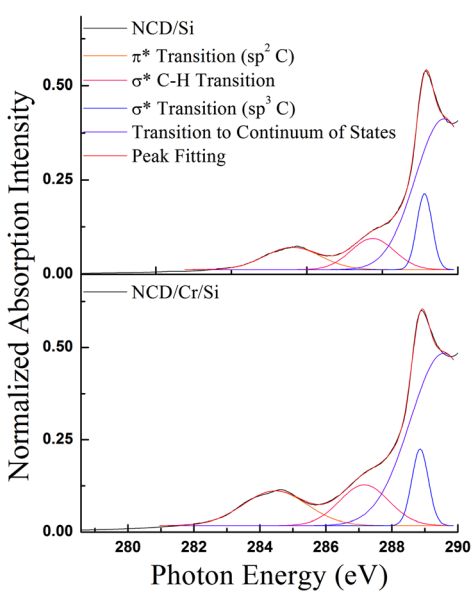

FIG. 4. NEXAFS experimental and deconvoluted spectra of the pre-edge and edge region of NCD on chromium coated silicon.

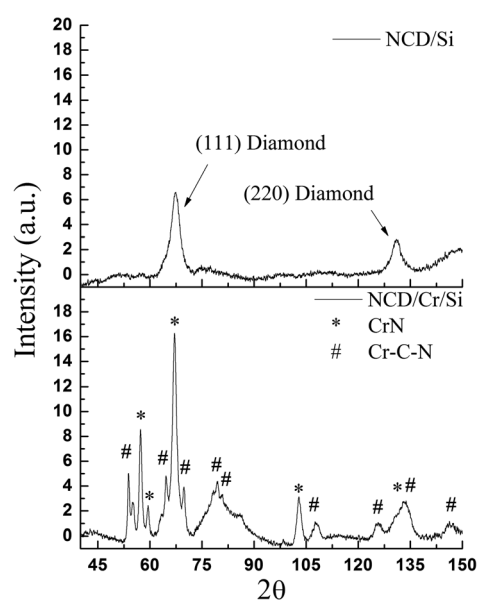

FIG. 5. XRD patterns for NCD grown on silicon (NCD/Si) and chromium coated silicon (NCD/Cr/Si).

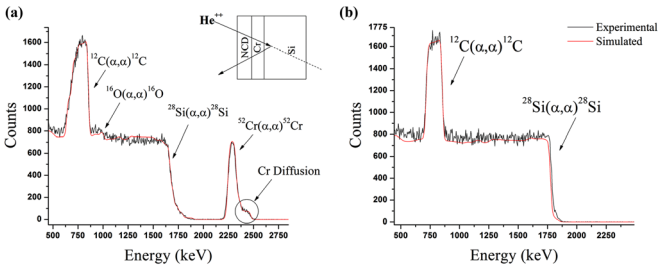

FIG. 6. NRBS of films deposited on chromium underlayer (a) and silicon (b) and highlighting chromium diffusion (a).

used is illustrated as an inset in Figure 6(a). The NRBS experimental spectrum along with the overlapped simulation spectrum is also shown in Figure 6(a). Simulation of the experimental spectrum was performed utilizing the n-Simplex algorithm implemented in SIMNRA.[38]

The chromium, silicon, and carbon edges are represented in the spectrum at the approximate energy values 2500, 1750 and 865 keV, respectively. The small peak appearing at approximately 990 keV is an oxygen peak which correlates with XRD detection of Cr_2O_3 in the film, confirming the presence of oxygen in the chromium peak layers. The trailing edge of the carbon peak (between 600 and 700 keV) and the leading energy edge of the chromium peak (between 2350 and 2500 keV) are showing signature broadening indicating interfacial mixing between the chromium layer and the film has occurred. By contrast, the film grown on silicon, Figure 6(b) displays nearly vertical, sharp, leading and trailing edges for both carbon and silicon. This indicates minimal or no interfacial mixing between the silicon substrate and the film.

The spread of the chromium underlayer, or its diffusion, is indicated by a circle in Figure 6(a). This trend decreases in terms of concentration from the underlayer towards the surface of the sample, from the chromium peak height at 2280 keV (30 at. % of chromium) to the leading edge at 2500 keV (1 at. % of chromium). Correspondence between the width of the carbon peak and extended shoulder from the chromium peak indicate the diffusion of chromium to the film surface.

AFM was used in this work to study the structural changes of the NCD films and also to understand the effect of underlayer. Figure 7 compares the grain size of the NCD films deposited on silicon substrate with and without chromium underlayer. The AFM topographical images show that the grain size of the film grown on chromium underlayer in Fig. 7(a) is larger than those of the silicon substrate without chromium in Fig. 7(b). The estimated grain size for the film grown on chromium (250 nm) is almost twice of that deposited on silicon substrate without a chromium underlayer (120 nm). RMS roughness based on AFM images taken for both samples revealed an increase in the roughness of the film grown on chromium over that grown on silicon; from 7.42 to 16.25 nm. The formation of different CrN and Cr-C-N phases may have resulted in the nucleation of larger grains on the film deposited on chromium coated silicon over that of the film deposited directly on silicon.

In addition to the increased grain size and roughness of film grown on chromium compared to that deposited on silicon, nanoindentation tests on both films also revealed a striking difference between the hardness and elastic moduli of these films. The load-displacement curves obtained from the nanoindentation tests on both films are shown in Figure 8. Interestingly, the curve obtained from the film deposited on silicon showed a lager variation during loading and unloading cycles, which is typically the signature of plastic deformation.[39] The film grown on silicon displayed a hardness and elastic modulus of 17.46 and 207.36 GPa, respectively. In contrast, the film grown on chromium displayed a much higher hardness and elastic modulus; 45.78 and 350.48 GPa. Theoretical simulations coupled with the experimental findings have predicted a decrease in the elastic modulus with the addition of nitrogen in the grain boundary region under various conditions; however, the experimental values in this study differ from the predicted values.[40–43] While these measurements show a contradiction from expected hardness values, the hardness of the film grown on chromium was much higher than that grown on silicon. This may be attributed to the formation of different hard phases (CrN, Cr-C-N, or C-N) in the films on chromium layer. The addition of Cr-C-N and CrN phases of molecular chromium may be a contributing factor to the greater hardness of the film grown on chromium. As a comparison, CrN alone has a reported hardness of approximately

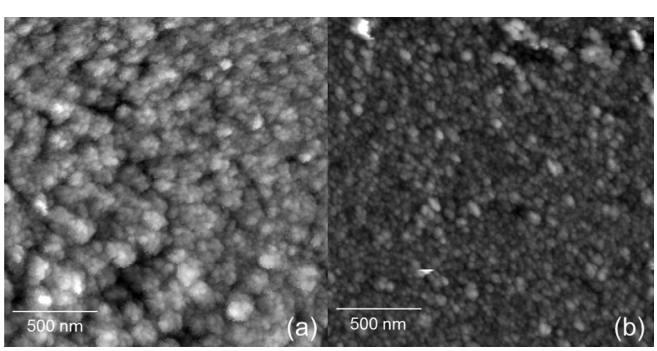

FIG. 7. AFM topographical images of (a) NCD/Cr/Si sample and (b) NCD/Si sample.

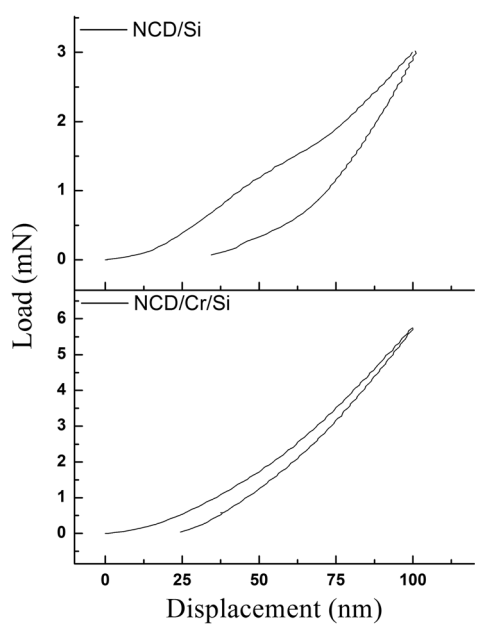

FIG. 8. Load-displacement curves for films grown on silicon (NCD/Si) and chromium coated silicon (NCD/Cr/Si).

19.6 GPa (Ref. 44), while the reported value for Cr-C-N ranges between 22.5 and 24.5 GPa.[45,46]

In summary, these investigations focused on NCD film characteristics for samples deposited on a single crystal silicon substrate with and without a chromium underlayer. Spectroscopic analysis clearly showed the formation of NCD structure in both films. However, bulk film analysis by XRD detected the presence of polycrystalline compounds of chromium, carbon and nitrogen; CrN and Cr-C-N; as well as chromium and oxygen (Cr_2O_3) indicating the presence of chromium and incorporation of nitrogen into those films. NRBS detected diffusion of the chromium underlayer through the film in correlation with XRD findings. AFM surface mapping determined a large increase in grain size and roughness over the film grown on silicon alone, and nanoindentation tests revealed that the hardness of the film grown on chromium is more than twice that of the sample grown on silicon. Faults in the film grown on silicon may have caused a kind of plastic deformation resulting in a lower than expected hardness.

Use of the Center for Nanoscale Materials (CNM) was supported by the U. S. Department of Energy, Office of Science, and Office of Basic Energy Sciences, under Contract No. DE AC02-06CH11357. A portion of the research was performed using EMSL, a national scientific user facility sponsored by the Department of Energy's Office of Biological and Environmental Research, located at Pacific Northwest National Laboratory (PNNL). PNNL is operated for the U.S. DOE by Battelle Memorial Institute under Contract No. DE-AC05-76RL01830. We would also like to acknowledge the staff at the Electron Microbeam Analysis Laboratory for their assistance in performing nanoindentation tests.

[1]T. Zimmerman, K. Janischowsky, A. Denisenko, F. J. Hernández Guillén, M. Kubovic, D. M. Gruen, and E. Kohn, Diamond Relat. Mater. **15**, 203 (2005).
[2]M. Amaral, P. S. Gomes, M. A. Lopes, J. D. Santos, R. F. Silva, and M. H. Fernandes, J. Nanomater. **2008**, 894352 (2008).
[3]Z. Cao and D. Aslam, Diamond Relat. Mater. **19**, 1263 (2010).
[4]S. Ohmagari and T. Yoshitake, Appl. Phys. Express **5**, 065202 (2012).
[5]D. M. Gruen, Annu. Rev. Mater. Sci. **29**, 211 (1999).
[6]M. Hajra, C. E. Hunt, M. Ding, O. Auciello, J. Carlisle, and D. M. Gruen, J. Appl. Phys. **94**, 4079 (2003).
[7]J. Phillip, P. Hess, T. Feygeison, J. E. Butler, S. Chattopadhyay, K. H. Chen, and L. C. Chen, J. Appl. Phys. **93**, 2164 (2003).
[8]H. C. Chen, K. F. Liu, N. H. Tai, W. F. Pong, and I. N. Lin, Diamond Relat. Mater. **19**, 134–137 (2010).
[9]N. N. Naguib, J. W. Elam, J. Birrell, J. Wang, D. S. Grierson, B. Kabius, J. M. Hiller, A. V. Sumant, R. W. Carpick, O. Auciello, and J. A. Carlisle, Chem. Phys. Lett. **430**, 345–350 (2006).
[10]Y. Avigal, O. Glozman, I. Etsion, G. Halperin, and A. Hoffman, Diamond Relat. Mater. **6**, 381–385 (1997).
[11]C. Bareiss, M. Perle, S. M. Rosiwal, and R. F. Singer, Diamond Relat. Mater. **15**, 754–760 (2005).
[12]J. G. Buijnsters, P. Shankar, W. Fleischer, W. J. P. van Enckevort, J. J. Schermer, and J. J. ter Meulen, Diamond Relat. Mater. **11**, 536–544 (2002).
[13]M. Korzynski, A. Pacana, and J. Cwanek, Surf. Coat. Technol. **203**, 1670–1676 (2009).
[14]J. G. Buijnsters, F. M. van Bouwelen, J. J. Schermer, W. J. P. van Enckevort, and J. J. ter Meulen, Diamond Relat. Mater. **9**, 341–345 (2000).
[15]V. P. Godbole, R. Narayan, Z. Xu, J. Narayan, and J. Sankar, Mater. Sci. Eng., B **58**, 251–257 (1999).
[16]N. V. Novikov, A. I. Borimsky, P. A. Nagorny, V. G. Delevi, and T. Yu Chipenko, Diamond Relat. Mater. **10**, 1602–1606 (2001).
[17]O. Glozman and A. Hoffman, Diamond Relat. Mater. **6**, 1847 (1997).
[18]O. Glozman, G. Halperin, I. Etsion, A. Berner, D. Shectman, G. H. Lee, and A. Hoffman, Diamond Relat. Mater. **8**, 859 (1999).
[19]R. Locher, C. Wild, N. Herres, D. Behr, and P. Koidl, Appl. Phys. Lett. **65**, 34 (1994).
[20]H. Chatei, J. Bougdira, M. Remy, P. Alnot, C. Bruch, and J. K. Kruger, Diamond Relat. Mater. **6**, 107 (1997).
[21]A. Badzian, T. Badzian, and S. T. Lee, Appl. Phys. Lett. **62**, 3432 (1993).
[22]S. Jin and T. D. Moustakes, Appl. Phys. Lett. **65**, 403 (1994).
[23]Y. Feng, Z. Zhou, Y. Zhou, and G. Zhao, Nucl. Instr. Meth. B **86**, 225–230 (1994).
[24]W. C. Oliver and G. M. Pharr, J. Mater. Res. **7**, 1564–1583 (1992).
[25]A. C. Ferrari and J. Robertson, Phys. Rev. B **61**, 14095 (2000).
[26]R. E. Schroder, R. J. Nemanich, and J. T. Glass, Phys. Rev. B **41**, 3738 (1990).
[27]D. S. Knight and W. B. White, J. Mater. Res. **4**, 385 (1989).
[28]P. Achatz, J. Garrido, M. Stutzmann, O. A. Williams, D. M. Gruen, A. Kromka, and D. Steinmueller, Appl. Phys. Lett. **88**, 101908 (2006).
[29]J. Birrell, J. E. Gerbi, O. Auciello, J. M. Gibson, and J. A. Carlisle, Dia. Relat. Mater. **14**, 86–92 (2006).
[30]F. L. Coffman, R. Cao, P. A. Pianetta, S. Kapoor, M. Kelly, and L. J. Terminello, Appl. Phys. Lett. **69**, 568 (1996).
[31]S. Osswald, G. Yushin, V. Mochalin, S. O. Kucheyev, and Y. Gogotsi, J. Am. Chem. Soc. **128**, 11635–11642 (2006).
[32]A. V. Sumant, P. U. P. A. Gilbert, D. S. Grierson, A. R. Konicek, M. Abrecht, J. E. Butler, T. Feygelson, S. S. Rotter, and R. W. Carpick, Dia. Relat. Mater. **16**, 718–724 (2007).
[33]J. T. Titantah and D. Lamoen, Phys. Rev. B **72**, 193104 (2005).
[34]Natl. Bur. Stand. (U.S.), Circ. **539**, VII 5 (1953).
[35]P. Ettmayer, Monatsch. Chem. **97**(4), 1248–1257 (1966).
[36]R. Kieffer, P. Ettmayer, and F. Petter, Monatsch. Chem. **102**(5), 1182–1196 (1971).
[37]H. McMurdie, M. Morris, E. Evans, B. Paretzkin, W. Wong-Ng, and Y. Zhang, Powder Diffr. **2**, 45 (1987).
[38]M. Mayer, *SIMNRA User's Guide*, Report No. IPP 9/113, Max-Planck-Institut für Plasmaphysik, Garching, Germany, 1997.
[39]D. Ge, A. M. Minor, E. A. Stach, and J. W. Morris, Jr., Philos. Mag. **86**, 4069–4080 (2006).
[40]J. T. Paci, T. Belytschko, and G. C. Schatz, Phys. Rev. B **74**, 18112 (2006).
[41]L. Shen and Z. Chen, Solids Struct. **44**, 3379–3392 (2007).
[42]J. Birrell, J. E. Gerbi, O. Auciello, J. M. Gibson, D. M. Gruen, and J. A. Carlisle, J. Appl. Phys. **93**, 5606 (2003).
[43]M. G. Fyta, G. C. Hadjisavvas, and P. C. Kelires, Dia. Relat. Mater. **16**, 1643–1647 (2007).
[44]H. Ichimura and Y. Ishii, Surf. Coat. Technol. **145**, 94–100 (2001).
[45]M. Cekada, M. Maček, D. K. Merl, and P. Panjan, Thin Solid Films **433**, 174–179 (2003).
[46]H. Pengfei and J. Bailing, Vacuum **85**, 994–998 (2011).